energies

Article

Electromagnetic Performance Investigation of Rectangular-Structured Linear Actuator with End Ferromagnetic Poles

Zahoor Ahmad [1,*], Basharat Ullah [1], Faisal Khan [1], Shafaat Ullah [2,*] and Irfan Sami [3]

1 Department of Electrical and Computer Engineering, COMSATS University Islamabad, Abbottabad 22060, Pakistan; basharat.bigb@gmail.com (B.U.); faisalkhan@cuiatd.edu.pk (F.K.)
2 Department of Electrical Engineering, University of Engineering and Technology Peshawar, Bannu Campus, Bannu 28100, Pakistan
3 School of Electrical and Electronics Engineering, Chung-Ang University, Dongjak-gu, Seoul 06974, Republic of Korea; irfansamimwt@gmail.com
* Correspondence: zahoorahmad9027@gmail.com (Z.A.); engr.shafaat@uetpeshawar.edu.pk (S.U.)

Abstract: Saving energy from domestic appliances is a focus in the effort to combat energy challenges. Linear compressors are a more efficient alternative to the traditional compressors used in refrigerators, which account for 20–40% of all residential electricity use. This article investigates the new topology of the moving magnet (MM), dual-stator single-mover linear oscillating actuator (DSSM-LOA) for linear compressor application. Both the stators were C-shaped, with coils looped across their end sides. Two permanent magnets (PMs) that were axially magnetized were housed on the mover. The PM structural shape significantly affected its fabrication cost and magnitude of magnetic flux density (B). The DSSM-LOA makes use of axially magnetized rectangular-shaped PMs because they are inexpensive and generate high electromagnetic (EM) force density. End ferromagnetic core materials were used to improve the magnetic flux, linking from the stator to the mover. All the design parameters were optimized through parametric analysis using the finite parametric sweep method. Parameters present within the three primary parameters (length, height, and depth) that were assumed constants were optimized, and the optimal dimensions were selected based on the EM force. The investigated DSSM-LOA was contrasted with traditional LOA designs, and they showed significant improvement in EM force per ampere, generally named motor constant (MC), MC per PM mass, MC density, cogging force, and stroke. Additionally, the proposed DSSM-LOA had a simple structure and low cost, and it operated in a feasible range of strokes for linear compressor application.

Keywords: actuator; dual stator; electromagnetic force; linear oscillation; planar structure

Citation: Ahmad, Z.; Ullah, B.; Khan, F.; Ullah, S.; Sami, I. Electromagnetic Performance Investigation of Rectangular-Structured Linear Actuator with End Ferromagnetic Poles. *Energies* **2023**, *16*, 5758. https://doi.org/10.3390/en16155758

Academic Editors: Guang-Jin Li and Xiao Chen

Received: 23 June 2023
Revised: 23 July 2023
Accepted: 31 July 2023
Published: 2 August 2023

1. Introduction

Linear compressors use linear motors instead of the traditional rotary motors found in conventional compressors. This technology allows for better control of compression and refrigerant flow, resulting in improved efficiency. It minimizes energy waste by eliminating the frequent on–off cycling that occurs with traditional compressors. They can maintain a more stable temperature inside the refrigerator, which reduces energy consumption and enhances efficiency. Manufacturers can significantly reduce energy consumption by incorporating linear compressor technology into refrigerators. Numerous modern refrigerators already use these energy-efficient compressors, contributing to reducing residential electricity consumption and combating energy challenges.

LOA is an electromechanical device that produces a regulated linear oscillating EM force in a predetermined stroke range [1]. The frequency of the oscillations of the EM force is controlled by varying the frequency of the alternating input loading. LOA typically functions on a resonance frequency. The mover mass and stiffness of the springs associated with the mover can be used to calculate the LOA's operating frequency [2]. Due to design restrictions, mover mass cannot be reduced so far, while spring stiffness can be altered. However, by applying specialized optimization techniques, mover mass can be lowered to a certain level while preserving performance indices, such as EM force and stroke [3]. When an actuator comes to functionality, resonance frequency operation performs efficiently. At the resonance frequency, the voltage difference between the applied voltage and the back EMF is at its lowest value, which results in the least amount of current passing through the coil. The input power to the LOA determines the mover extreme point of oscillation, known as the stroke of the LOA. The consequence of the high input power is more copper loss, which further reduces the efficiency of the LOA [4,5].

There are two parts of the LOA; one is static (stator), and the other is moving (mover). The stator produces a controlled magnetic field, and the active part of the mover aligns itself with it. The mover adjusts its position, due to the alignment of its active parts. Linear oscillation is produced by employing mover position adjustment [6,7].

The LOA's geometry is often either planar- or tubular-shaped. The tubular shape is well compacted, has no end-winding effect, and provides a high EM force [8]. In contrast, the PM price of a tubular shape is higher than the rectangular PM because of additional fabrication costs and material waste. Furthermore, a rectangular PM structure of the needed size is simple to acquire, whereas a tubular PM structure of the required dimension cannot be accomplished by attaching numerous small-dimensioned PMs [9]. Additionally, more consequences of the tubular shape arise when manufacturing the core materials lamination. Conventionally, rotary motors are laminated axially, while LOAs are laminated radially to reduce core losses. The consequences of radial lamination of LOA are a small stacking factor and reduced air-gap flux density. A new method was analyzed in [10], which focused on enhancing the stacking factor and air-gap flux density by designing the stator pole end and back iron in separate formations. To reduce the mover core losses, a scheme of making groves was investigated in [11]. This formation scheme reduced the mover core losses significantly. In addition, by increasing the number of groves, the response of the linear actuator in terms of mover core losses decreased linearly. Therefore, the mover structure of the rectangular LOA is feasible for making more lamination sheets.

LOAs are categorized according to the components of the mover: moving coils, moving iron, and moving magnets [12–14]. Regarding cost, moving coil LOA is better but challenging when the moving part is electrically loaded. Furthermore, the LOA of a moving coil does not result in the same EM force as that of a moving magnet. Moving iron LOA is cost-effective, since their mover is not composed of PM or winding. There is a greater mass associated with the mover of moving iron LOA. On the other hand, the advantages of moving magnet LOA include good EM force, high magnetic field density, and greater efficiency. Additionally, on account of the lower value of the mover mass, the operating resonance frequency is high, generating a greater output power, and the mass flow rate is high as well [15].

A two-stator, one-mover-dual-stator modular topology was examined [16]. Due to the placement of the second stator inside the tubular mover and the encapsulation of the one stator surrounding it, a high thrust force density was achieved. Detent force, the sum of the cogging force, and the end force were comprehensively analyzed in [17]. This unwanted factor of the LOA was minimized significantly by using the finite parametric sweep method. PMs positioned at the mover end of an LOA design have the disadvantage of being PMs exposed to the air because of the LOA open structure. A tubular-shaped LOA with a Halbach array configuration of the PMs placed at the mover ends was analyzed in [18], and its performance was improved using end ferromagnetic poles. LOA can be utilized for a variety of fast-moving applications, including robotics, electric hammers, bio-medical equipment, and compressors [19,20].

This article presents a moving magnet planar topology called DSSM-LOA developed for a linear compressor application. A brief explanation of mechanical design and illustrations of its two- and three-dimensional (3-D) structures are given. Details of the operating principles are discussed. A single-stator single-mover (SSSM) LOA was initially constructed, and its design parameters were optimized by parametric analysis utilizing the finite parametric sweep approach. The second stator was built on the other side of the mover using optimized parameter dimensions. The performance of the proposed DSSM-LOA was presented, including the contribution of the end ferromagnetic core material in B. Additionally, output parameters, such as EM forces and cogging forces of the conventional dual-stator (Con-DS) LOA, proposed SSSM-LOA, and DSSM-LOA, were compared to demonstrate the superiority of the proposed DSSM-LOA. Finally, the performance of the proposed DSSM-LOA was compared with the state-of-the-art designs of the LOA regarding MC, stroke, MC density, and MC per PM mass.

2. Mechanical Design and Principle of Operation

The two-dimensional (2-D) structures of the presented SSSM-LOA and DSSM-LOA are depicted in Figure 1a,b, respectively. The stator part of the investigated LOA comprised coils and core materials. Coils were looped across the ends of the C-shape. To improve the flow of magnetic flux, pole shoes were attached to the C-shape's ends. The mover of the investigated LOA was composed of two PMs and core materials. PMs were axially magnetized, and their magnetization directions were opposite to one another. Core materials were placed between the PMs, which provided the least reluctance path for magnetic flux to flow from one stator pole to the corresponding stator poles. Core materials at the mover ends helped to reduce leakage flux and provided ease to the magnetic flux, linking from the stator to the mover. Figure 1a demonstrates SSSM-LOA, which was composed of one stator and a mover. A stator with exact parameter dimensions was constructed on the opposite side of the first stator, as shown in Figure 1b. Figure 1b demonstrates DSSM-LOA, where the mover was placed between the two stators.

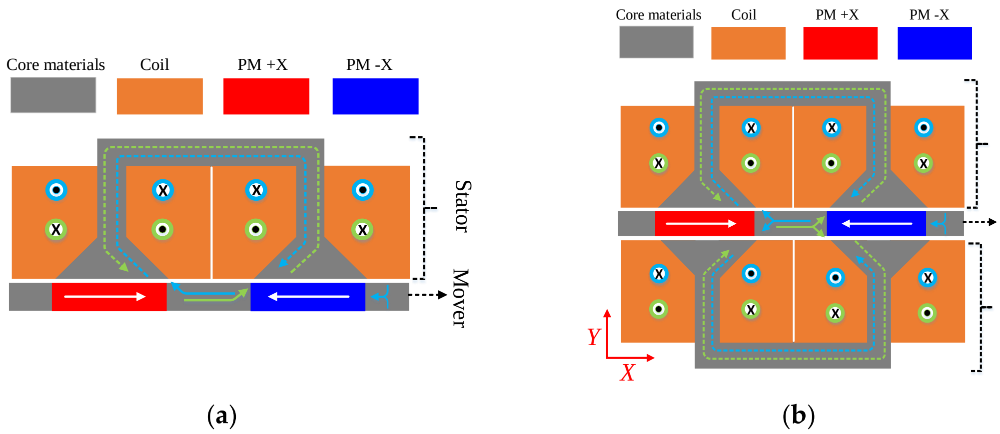

Figure 1. The 2-D design topology of the investigated LOA. (**a**) SSSM-LOA; (**b**) DSSM-LOA.

The proposed DSSM-LOA coils of each stator pole were excited in the opposite directions of the current to provide uni-directional magnetic flux in the stator core. Similarly, the direction of the current through the second stator was opposite to that of the first stator. Magnetic flux flowed in the direction indicated by the arrows when the coils were powered up with the direction of the current depicted by the symbols, as seen in Figure 2. The mover oscillated between two extreme points along the x-axis. The $-x$ extreme position of the mover is shown in Figure 2a. The mover moved to the maximum negative position ($-x$) when the stator coil current flowed in the direction depicted in Figure 2a. The phenomenon of the magnetic flux passing through the path, encountering the least reluctance, caused the EM force to be applied to the mover. As a result, the mover received an EM force along the $-x$ direction to produce the least reluctance route. Similar phenomena happened when the current direction was altered, as illustrated in Figure 2b. In the opposite direction of the current, the mover displaced to the $+x$ extreme position. The proposed DSSM-LOA operated on a single-phase alternating current (AC): during the first half-cycle of the current, the mover shifted to the one extreme position, and during the second half-cycle, it shifted to the other extreme position. Hence, the mover oscillation frequency became equal to the input loading frequency. The three-dimensional (3-D) structure of the investigated DSSM-LOA is shown in Figure 3, where Figure 3a illustrates the compact view, and Figure 3b demonstrates the cut view to show the inner structure (sections) of the DSSM-LOA. To reveal the 3-D structure of each part of DSSM-LOA, the exploded view is shown in Figure 3c. The optimum dimensions of each parameter of the investigated DSSM-LOA are shown in Table 1. Materials assigned to different regions of the proposed design during FEM are illustrated in Figure 4 and Table 2. The regions of the PMs that were represented by *R21* and *R23* were initially air; then, a specified condition of using the remanent flux density of magnitude 1.3 T was used in the magnetic field module. The direction of the magnetic flux of PM region *R21* was set along the $-x$-axis, and the direction of *R23* was defined along the $+x$ axis.

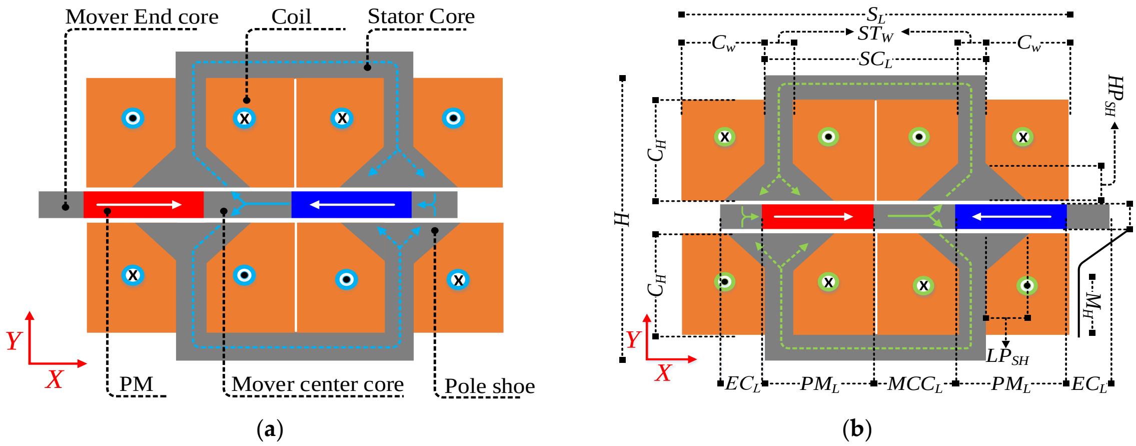

Figure 2. The 2-D design topology of the examined LOAs at their end points of the mover. (**a**) $+x$ end point; (**b**) $-x$ endpoint.

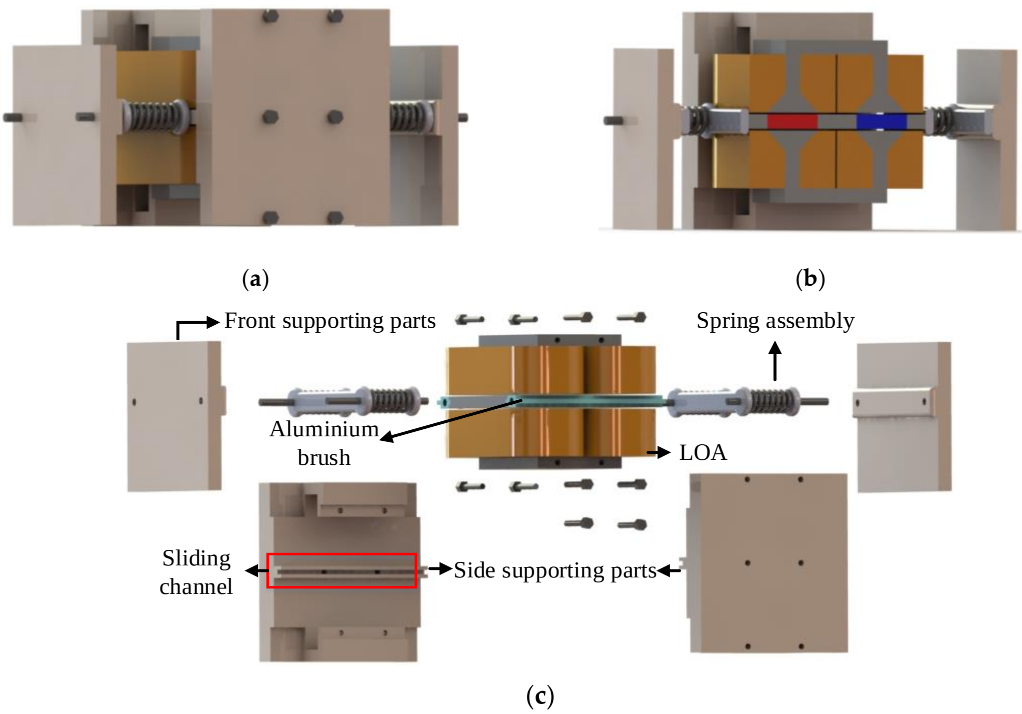

Figure 3. The 3-D views of the DSSM-LOA. (**a**) Compacted view; (**b**) cut view; (**c**) unpacked (exploded) view.

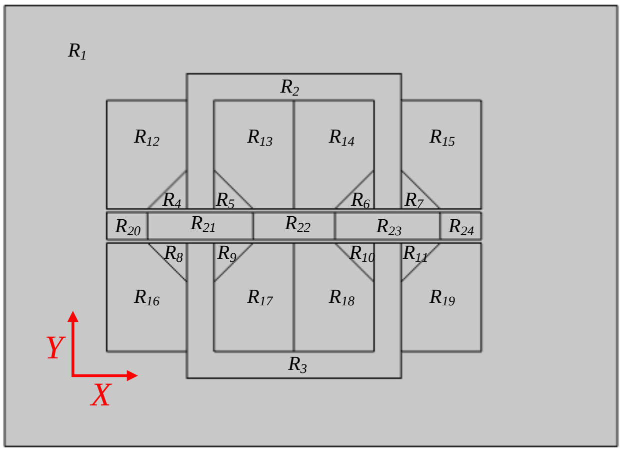

Figure 4. The 2-D view during FEM analysis.

Table 1. Optimum dimensions of the DSSM-LOA.

Parameter Description	Symbol	Value (mm)
Height of DSSM-LOA	H	90
Depth of the DSSM-LOA	-	120
Stator length of DSSM-LOA	S_L	110
Coil width	C_w	22
Coil height	C_H	32
Stator core length	SC_L	66
Stator tooth width	ST_W	11
Height of the pole shoe	HP_{SH}	10
Length of the pole shoe	LP_{SH}	10
Mover height	M_H	8
Mover center core length	MCC_L	24
Mover end core length	EC_L	12
PM length	PM_L	31
PM height	-	8
Air gap	-	1

Table 2. Materials used during FEM for different regions of the proposed design.

Region	LOA Part	Material
R_1	Environment	Air
R_2, R_3	Stator core	Low carbon steel 1010
R_4, R_5, R_6, R_7, R_8, R_9, R_{10}, R_{11}	Pole shoe	Low carbon steel 1010
R_{12}, R_{13}, R_{14}, R_{15}, R_{16}, R_{17}, R_{18}, R_{19}	Coils	Copper
R_{20}, R_{24}	Mover end core	Low carbon steel 1010
R_{22}	Mover center core	Low carbon steel 1010
R_{21}, R_{23}	PMs	Air plus remanent flux density (1.3 T) condition

3. Parametric Analysis

The proposed LOA was optimized through magneto-static conditions using the direct current (DC) and the finite element parametric sweeping method, and the optimum value of the parameter under investigation was selected based on the EM force. The optimum value was verified for both DC directions of value $5A$. SSSM-LOA, shown in Figure 1a, was initially designed, and its parameter dimensions were optimized using the finite parametric sweep method. SSSM-LOA comprised one stator, placed to the side, and a mover. While designing DSSM-LOA, the parameter dimensions of the second stator were selected equal to the optimized parameters of the stator of SSSM-LOA. The DSSM-LOA's stator length

(S_L), height (H), and depth (D) were kept constant to maintain a constant volume, while parameters inside the geometry were kept varied. The mover length was kept constant, and its value was kept equal to the stator length (S_L). EM force was analyzed at a mover mid-position and extreme position as well.

The parameters of the LOA for which the parametric optimization was accomplished and discussed briefly are illustrated in Figure 5. Coil height (C_H) was optimized by changing its value toward the back core height, as shown by the cyan color in Figure 5. The arrow of this line shows the direction toward which the coil height value was changed. Coil width (C_W) value was varied toward the stator tooth width (ST_w), as shown by the blue arrow. Permanent magnet length (PM_L) was also varied toward the center core, which is illustrated by the green color. Similarly, all the other parameters were optimized by using the parametric sweep methodology. The effects of C_H, ST_w, and PM_L on EM force and the dimension of the corresponding other parameter will be discussed in the coming section.

The investigated design of DSSM-LOA produced an EM force, due to the interaction of the PM magnetic field with the magnetic field produced by the coils. Since the magnetic field of the coil depended on the number of turns in the coil, the number of turns was kept updated by using the mathematical relation:

$$N_t = \left[\left(\frac{C_H \times C_W}{{T_D}^2}\right) - \frac{1}{2}\left(\frac{HP_{SH} \times LP_{SH}}{{T_D}^2}\right)\right] C_{F_f} \quad (1)$$

In (1), N_t is the turns number, C_H is the coil height value, C_L is the length of the coil, T_D is the single wire diameter, HP_{SH} is the pole shoe height, LP_{SH} is the pole shoe length, and C_{F_f} is the coil filling factor.

In Figure 6, the coil height (C_H) was optimized in terms of EM force and back core height. By increasing the value of C_H, the back core height dimension was reduced; hence, the back core height value was also optimized. Figure 6a demonstrates the impact of C_H on the EM force and back core height at a mean position of the mover. The impact of the C_H value on the EM force at the extreme position of the mover is illustrated in Figure 6b. Figure 6a shows that at the mover's mean position, the C_H, was optimum at 33 mm, whereas the coil height was optimum at 32 mm at the mover's extreme positions, as illustrated in Figure 6b. In a further investigation of the proposed design, the C_H value of 32 mm was selected to design the LOA for high stroke value.

Stator tooth width was optimized in terms of EM force and coil width (C_w), as shown in Figure 7. To maintain the overall length at a constant and develop an effect of C_w on the stator tooth width ST_w, a specified mathematical condition was used in the parameter definition portion, which was:

$$S_L = 2(C_w + ST_w) \quad (2)$$

$$C_w = 1/2(55[\text{mm}] - ST_w) \quad (3)$$

A parametric sweep was used on ST_w, which affected the value of the C_w, and there was no effect on the value of S_L. In this analysis, with the change in the value of C_w, the number of turns changed as well. Figure 7a shows how altering the values of the parameters affected the EM force at a mover mean position, which demonstrates that the optimal value of the ST_w was 8 mm. Figure 7b illustrates the EM force response of the proposed design at the mover extreme position for different values of C_w and ST_w. Figure 7b reveals that the optimum ST_w and C_w values were 11 mm and 22 mm, respectively. The overall length of the LOA was kept constant, and the value of the ST_w was made dependent on C_w. Hence, both ST_w and C_w were optimized in this optimization approach.

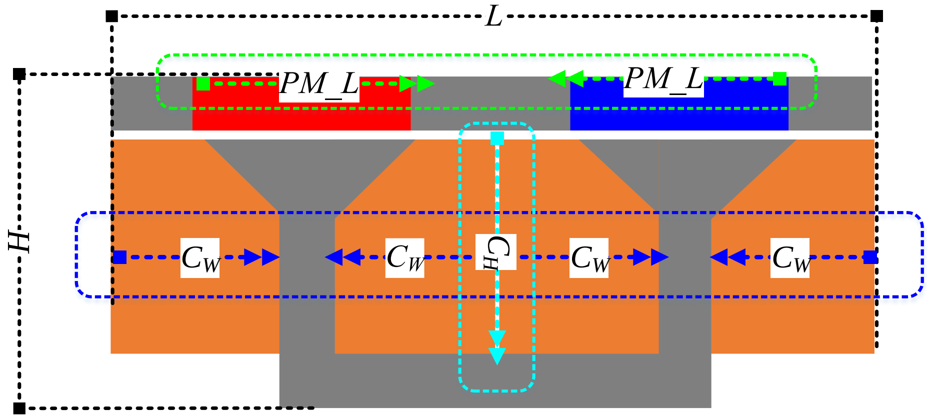

Figure 5. Illustration of fixed and optimized parameters of the SSSM-LOA.

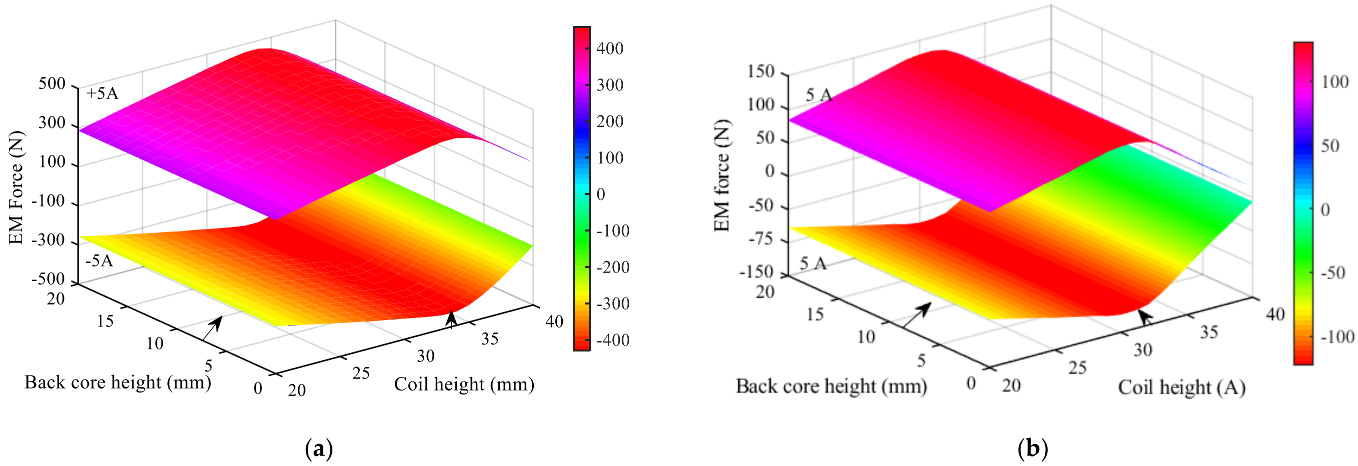

Figure 6. Parametric optimization by changing the parameters of coil height. (**a**) Mover's mean position; (**b**) extreme position of the mover.

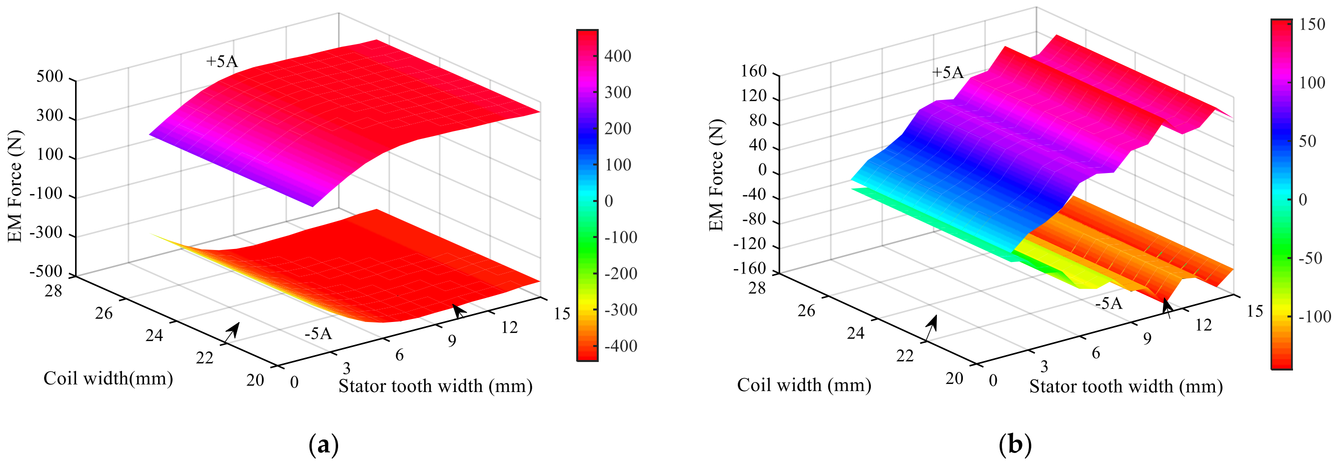

Figure 7. Parametric optimization by changing the parameters of coil length. (**a**) Mover's mean position; (**b**) extreme position of the mover.

Regarding EM force and stroke, the PM's end position and the length of the core materials between the PMs were also crucial. Therefore, an optimization approach regarding PM length (PM_L) and mover center core length was accomplished and is illustrated in Figure 8. The response of the parameter alteration in terms of average EM force through overall stroke is shown in Figure 8. Figure 8a demonstrates the effect of PM_L on EM force toward the $+x$ axis. For the opposite direction of the current, the impact of PM_L on EM force is illustrated in Figure 8b. This optimization approach revealed that PM_L of value 31 mm gave the optimum value, where the mover center core length was 24 mm.

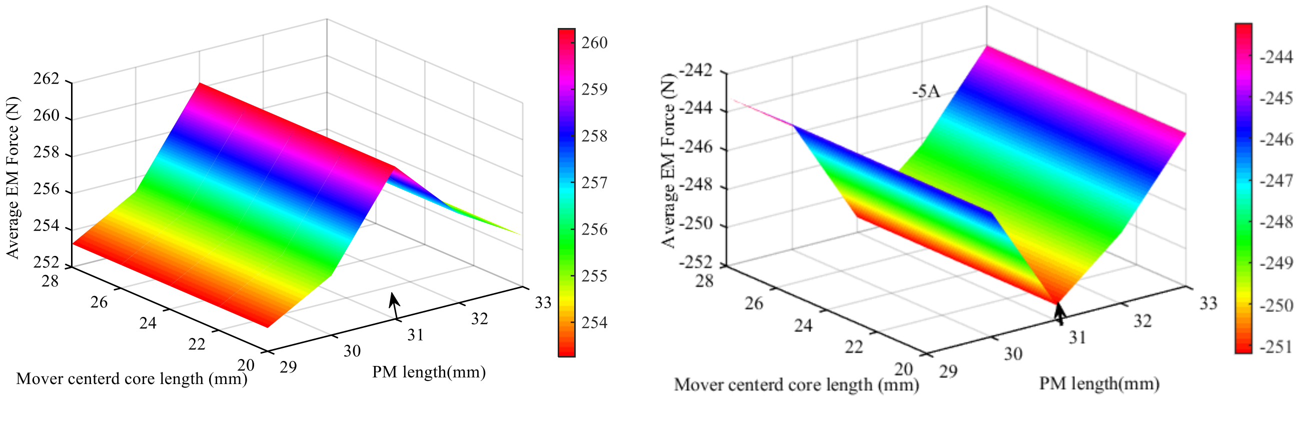

Figure 8. PM length optimization. (**a**) Average EM force response through overall stroke toward the $+x$ direction. (**b**) Average EM force response through overall stroke toward the $-x$ direction.

4. Mechanical Structures Comparison

The masses of several sections, including the ferromagnetic core materials, copper coils, and PMs materials, were compared between the proposed DSSM-LOA and the conventional one (Con-DS-LOA) investigated in [9]. Mechanical designs of Con-DS-LOA and the proposed DSSM-LOA are depicted in Figure 9a,b, respectively. The major difference between these designs was the DSSM-LOA coil was split and placed at the ends of the C-shaped stator core. Additionally, the proposed DSSM-LOA had pole shoes attached to both sides of the stator core, whereas the Con-DS-LOA used the pole shoe attached to one side of the stator core. Notably, the proposed DSSM-LOA had ferromagnetic materials attached to the ends of the mover, but the Con-DS-LOA did not have any end ferromagnetic core materials. The effects of the end ferromagnetic materials will be addressed in the section that follows. Calculated values of the masses used in different sections of the Con-DS-LOA and proposed DSSM-LOA are listed in Table 3.

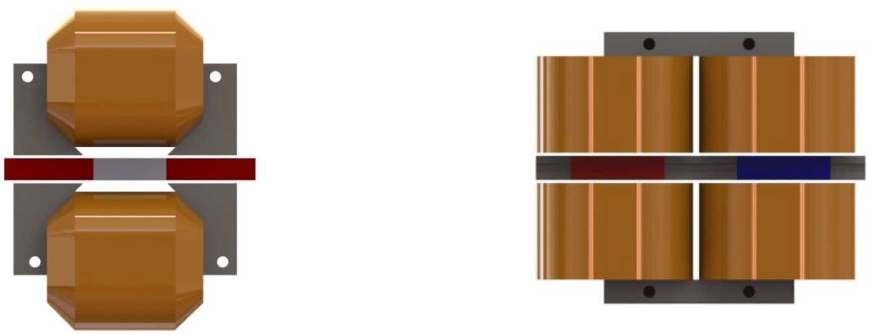

(**a**) (**b**)

Figure 9. Mechanical designs of LOA. (**a**) Con-DS-LOA [9]; (**b**) proposed DSSM-LOA.

Table 3. Mass comparison of different parts of the proposed DSSM-LOA and the Con-DS-LOA [9].

Design	Materials Description	Mass (Kg)
Con-DSLOA [9]	Core	2.254
	Copper	5.128
	PM	0.384
Proposed DSSM-LOA	Core	1.885
	Copper	5.410
	PM	0.298

5. FEM Results and Discussion

The proposed DSSM-LOA-simulated view at their extreme mover positions is shown in Figure 10. Figure 10a represents the mover's left extreme position (−10 mm stroke), where the right upper and lower stator coils were magnetized toward the $-y$ and $+y$ directions, respectively. Additionally, the left upper and lower stator coils were magnetized toward the $+y$ and $-y$ directions, respectively. The mover was displaced toward the $-x$ direction, and the mover center core was aligned with the stator core, due to which the magnetic flux lines completed their routes following the least reluctance path. Similarly, Figure 10b shows the proposed DSSM-LOA-simulated view, where the mover was displaced to the extreme right position (+10 mm stroke). The configuration of the coil magnetization direction in Figure 10b shows that the left upper and lower stator coils were magnetized toward the $-y$ and $+y$ axes, respectively. Similarly, the magnetization directions of the right upper and lower stator coils were opposite to the left stator coils.

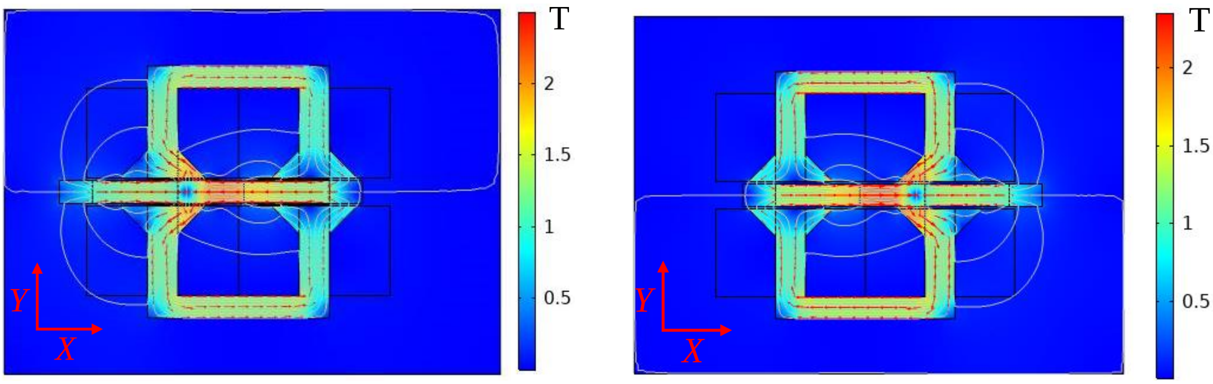

(**a**) (**b**)

Figure 10. Magnetic flux flow view. (**a**) Mover shifted toward the extreme left position; (**b**) mover shifted toward the extreme right position.

The magnetic flux linking the stator core to the mover-centered core is depicted in Figure 11. The proposed DSSM-LOA contained two stators, and each stator had two poles. The coil's magnetic flux lines entered the mover-centered core through one stator pole and then entered the other stator pole. Figure 11a represents the DSSM-LOA topology, where each pole was labeled based on its location. The magnetic flux lines entering the left upper and lower stator poles when the direction of the magnetic flux lines through the mover-centered core was from right to left are depicted in Figure 11b. Moreover, for the opposite direction of the stator coil current, the magnetic flux lines entering the right upper stator pole and right lower stator pole are also presented in Figure 11b.

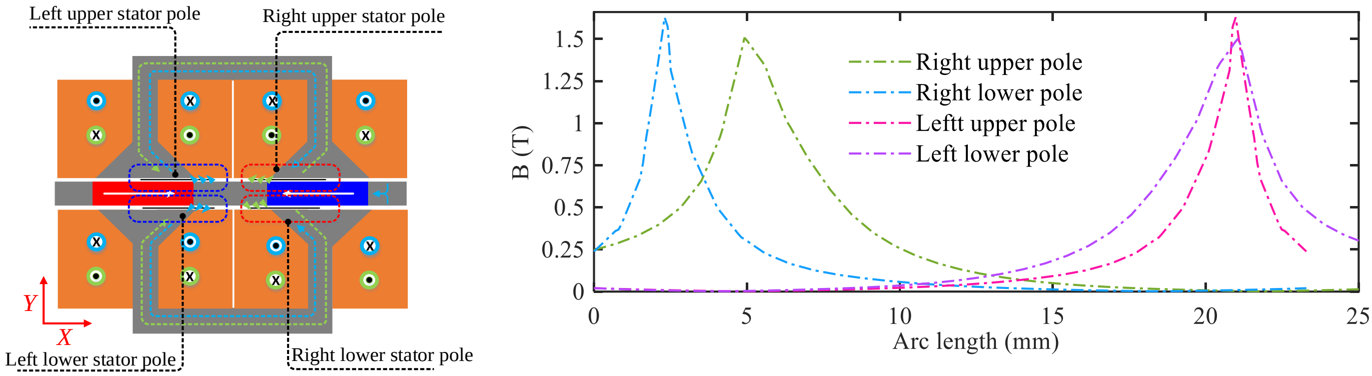

(**a**) (**b**)

Figure 11. Magnetic flux linking the mover core to the stator poles. (**a**) Representation of the LOA part where the magnetic flux density was measured. (**b**) Line graph of *B* in the air gap, measured in front of the stator pole.

The proposed LOA contained end ferromagnetic materials at both sides of the mover. Contribution in terms of magnetic flux lines, entering from the stator core to the mover end core and then entering to the PM south pole, was measured along a line and illustrated in Figure 12. The location of the line, along which *B* was measured, is shown in Figure 12a. The direction of the magnetic flux lines through the mover portion at this time was from the left to the right. Figure 12b depicts the magnetic flux lines entering the PMs from the left side with and without the presence of the core materials. Because of the ferromagnetic materials coupled to the mover, substantial magnetic flux was entering the PM south pole, as illustrated in Figure 12b.

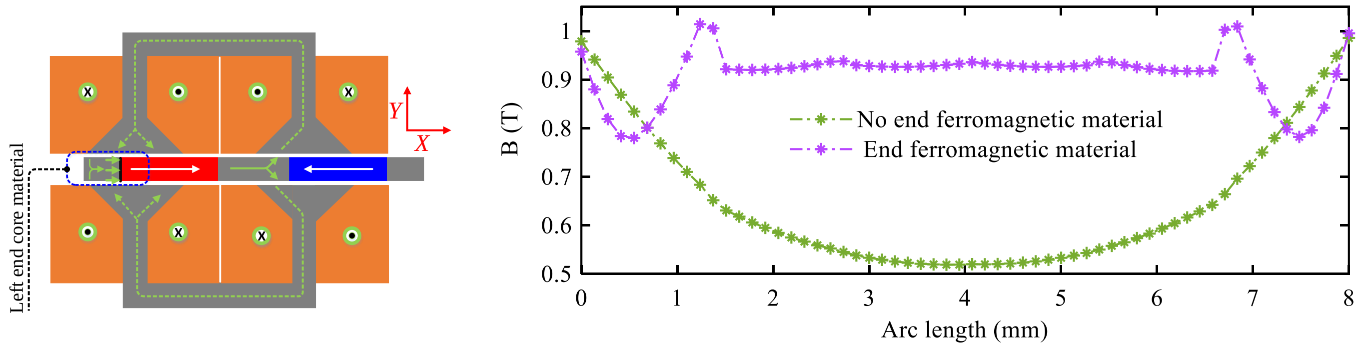

(**a**) (**b**)

Figure 12. Contribution of end ferromagnetic core materials in terms of *B* through the left mover end. (**a**) Representation of the LOA part, where *B* was measured. (**b**) Line graph of *B* with and without end ferromagnetic materials.

Similar to the previous analysis, the same investigation of magnetic flux, entering the mover from the right end, was accomplished and is presented in Figure 13. At this instant, the direction of magnetic flux lines through the mover part was from the right to the left. Magnetic flux due to the right-end ferromagnetic core part added to the magnetic flux of the PM. For ease of comprehension, Figure 13a shows the location where *B* was measured. A quantitative assessment of *B* in the presence and absence of core materials is depicted in Figure 13b. This analysis concluded that the end ferromagnetic core materials significantly reduced the leakage flux, which is the primary concern of planar topology.

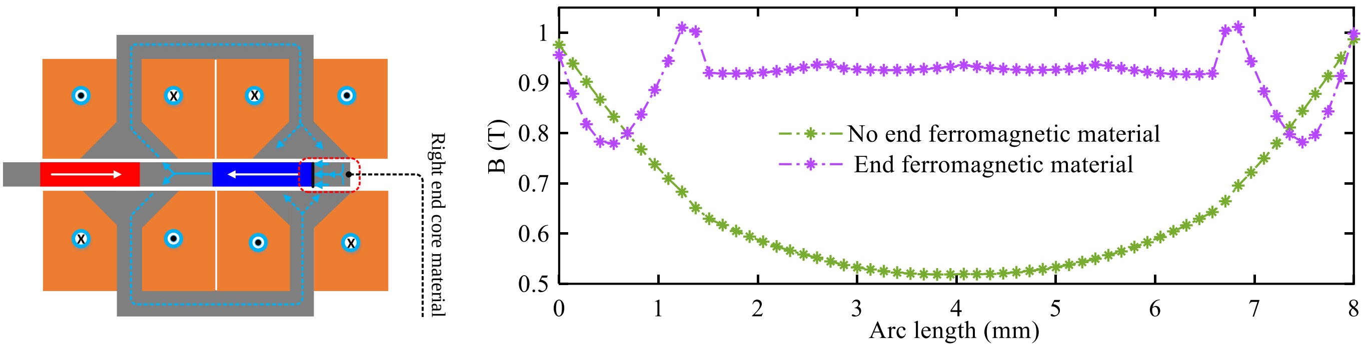

(**a**) (**b**)

Figure 13. Contribution of end ferromagnetic core materials in terms of B through the right mover end. (**a**) Representation of the LOA part, where B was measured. (**b**) Line graph of B with and without end ferromagnetic materials.

The EM force responses of Con-DS-LOA, proposed SSSM-LOA, and DSSM-LOA for different values and both directions of DC are depicted in Figure 14. The EM force displayed in the first quarter portion of Figure 14 displaced the mover from the mean position to the $+x$ extreme position. In contrast, the EM force plotted in the third quadrant shifted the mover from the mean position to the $-x$ extreme position. Since SSSM-LOA contained one stator component, its EM force value was less than that of DSSM-LOA. The slope of the line, representing the EM force for different input current values, demonstrated the actuator's motor constant (MC). EM force per ampere current of Con-DS-LOA was 120N/A, while the proposed SSSM-LOA and DSSM-LOA provided EM forces with MC values 64N/A and 132N/A, respectively.

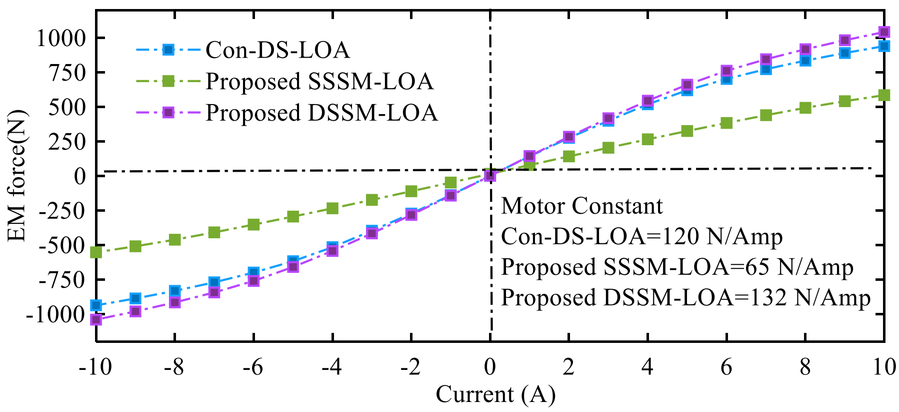

Figure 14. EM forces of Con-DS-LOA, proposed SSSM-LOA, and DSSM-LOA for different values and directions of input currents.

The EM forces of Con-DS-LOA and the presented DSSM-LOA at various mover positions within the intended stroke are depicted in Figure 15. Figure 15 is divided into four quadrants for ease of comprehension. The EM force shown in the second quadrant pushed the mover from the extreme $-x$ final point to the mid position, whereas the EM force shown in the first quadrant drove the mover even more to the extreme $+x$ position. As seen in the fourth and third quadrants of Figure 14, altering the current's direction caused the EM force's direction to reverse. In the fourth and third quadrants of Figure 15, the mover was shifted by EM forces from the final $+x$ point to the mean point and then to the extreme $-x$ point. Due to the bi-directional nature of single-phase alternating loading, the mover changed extreme points during the first half-cycle and returned to its original position during the second half of the cycle. This figure summarizes the EM force responses of the proposed DSSM-LOA and Con-DSSM-LOA, which indicate a significant improvement in terms of EM force.

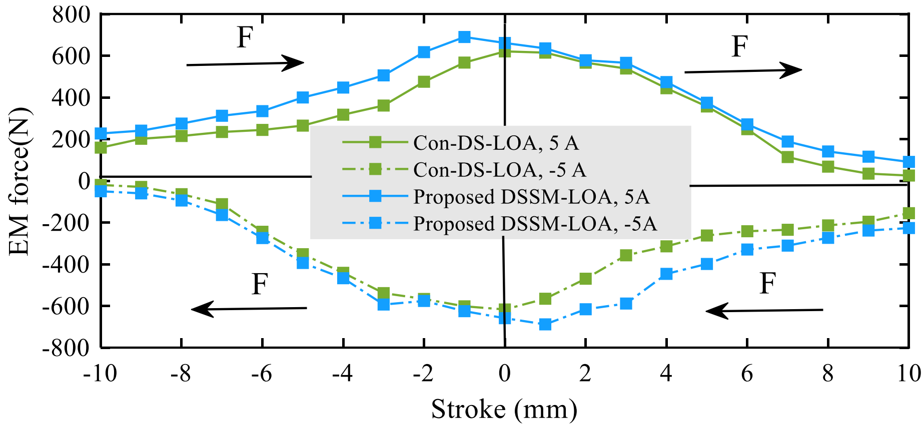

Figure 15. EM forces of Con-DS-LOA and proposed DSSM-LOA at different mover positions.

The cogging forces of Con-DS-LOA, proposed SSSM-LOA, and DSSM-LOA were examined and are shown in Figure 16. Because SSSM-LOA had only one stator and a mover, a strong attraction existed between the stator and mover. Con-DS-LOA and DSSM-LOA both had two stators that were offset from the mover. As a result, some force components canceled one another, resulting in lower cogging force values.

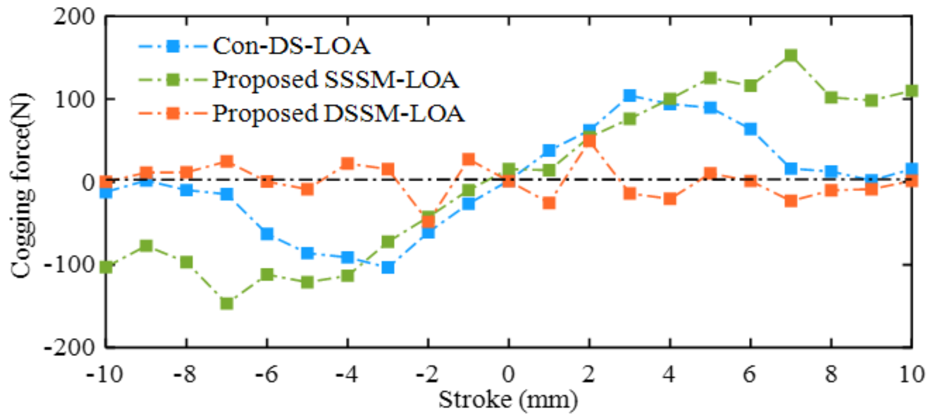

Figure 16. Cogging forces of Con-DS-LOA, proposed SSSM-LOA, and DSSM-LOA at different mover positions.

The SSSM-LOA time-dependent EM force response was examined at distinct peak-to-peak magnitudes of an alternating current (AC) and is illustrated in Figure 17. An AC was energized to the stator coils during time-dependent EM force investigation. The mover position was kept fixed at the mean position. The response of the SSSM-LOA with regards to EM force was directly related to the AC peak-to-peak value. Similarly, the time-dependent EM force of DSSM-LOA was also examined for distinct values of the peak-to-peak AC. DSSM-LOA also showed a linear increase in EM force, which was analyzed for 1 A, 3 A, 5 A, and 7 A, as depicted in Figure 18. DSSM-LOA gave an EM force almost double that of SSSM-LOA. The time-dependent EM forces of Con-DS-LOA, SSSM-LOA, and DSSM-LOA were compared using 5 A peak-to-peak AC and are shown in Figure 19. The proposed DSSM-LOA provided a better EM force, compared to Con-DS-LOA and SSSM-LOA.

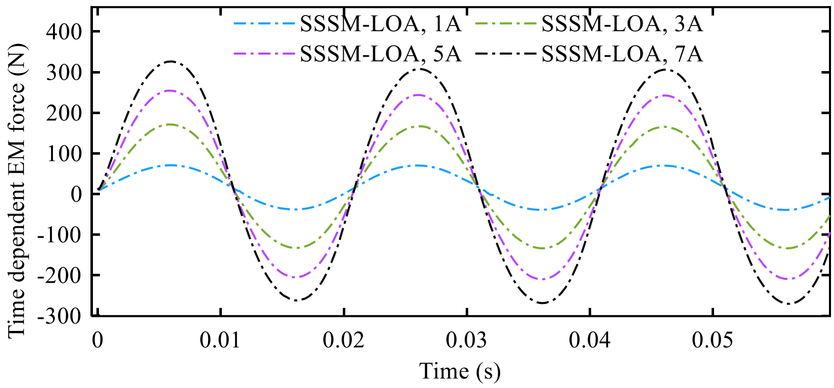

Figure 17. Time-dependent EM force of SSSM-LOA for different amplitudes of time-dependent input currents.

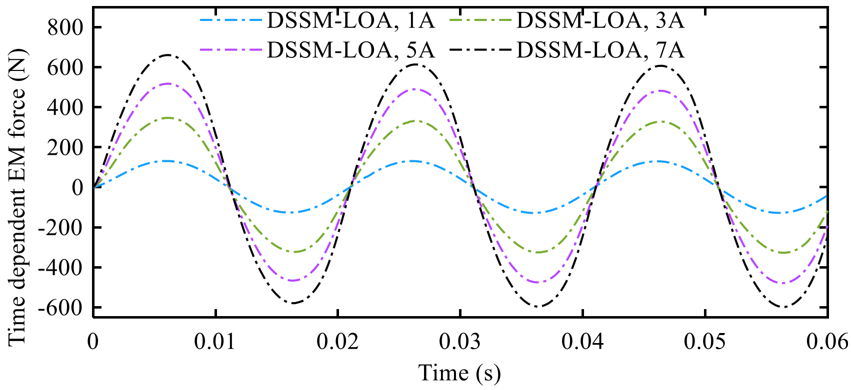

Figure 18. Time-dependent EM forces of DSSM-LOA for different amplitudes of time-dependent input currents.

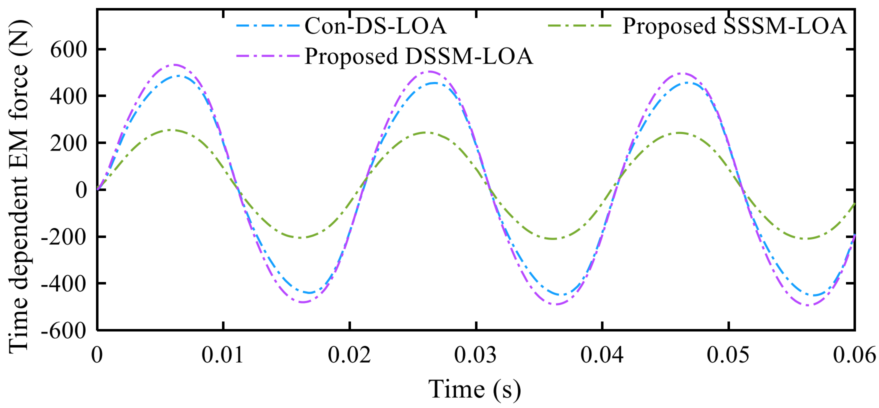

Figure 19. Comparison of time-dependent EM forces of Con-DS-LOA, SSSMLOA, and DSSM-LOA.

The FEM analysis of Con-DS-LOA and DSSM-LOA revealed that the EM force response of the proposed design was better than Con-DS-LOA. The MC of the Con-DS-LOA was 120N/A, while the proposed DSSM-LOA produced an EM force with an MC value of 132N/A. Moreover, the cogging force, which is an unwanted factor of an electric motor, was less in the proposed topology of DSSM-LOA. Furthermore, the time-dependent EM force of the proposed DSSM-LOA was also better, compared to the time-dependent EM force of Con-DS-LOA.

6. Thermal Analysis

Better thermal characteristics of an electric motor play a significant role in their fault-tolerance capabilities and life spans. Heat in an electric motor is generated due to copper and core losses. There has been significant improvement regarding the thermal management of electrical motors, such as liquid water-cooling methods, air-cooling methods, oil spray-cooling methods, etc. [21]. Another approach regarding thermal management is using insulating materials with a high thermal conductivity, better insulation ability, and capability to withstand high temperatures. A novel material with better heat conduction ability was introduced in [22]. Upon using this novel material, the power density of the motor was enhanced up to 50 percent with a normal range of temperature.

The thermal characteristics of the proposed DSSM-LOA were analyzed and are shown in Figure 20, where Figure 20a presents a front view, and Figure 20b illustrates a tilted view. This image presents the temperature distribution of the proposed DSSM-LOA after being placed under 10 h of operation. As seen in Figure 20, the coil and stator core, which had a temperature of around 76.5 °C, experienced the highest temperature increases.

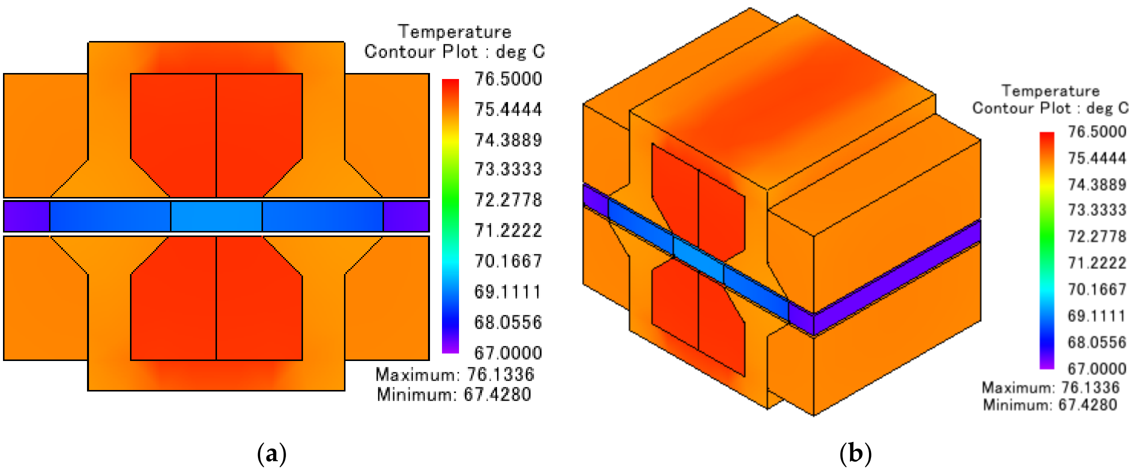

Figure 20. Thermal view of the proposed DSSM-LOA: (**a**) front view, (**b**) tilted view.

The temperatures of different DSSM-LOA components at various time intervals are shown in Figure 21. The components that were most affected by heat were the stator coils and core. The temperatures of all parts exhibited stable behavior after four hours of operation, and this stability was examined for up to ten hours. This analysis concluded that the temperature of the proposed design stabilized after a four-hour operation and reached 76.5 °C.

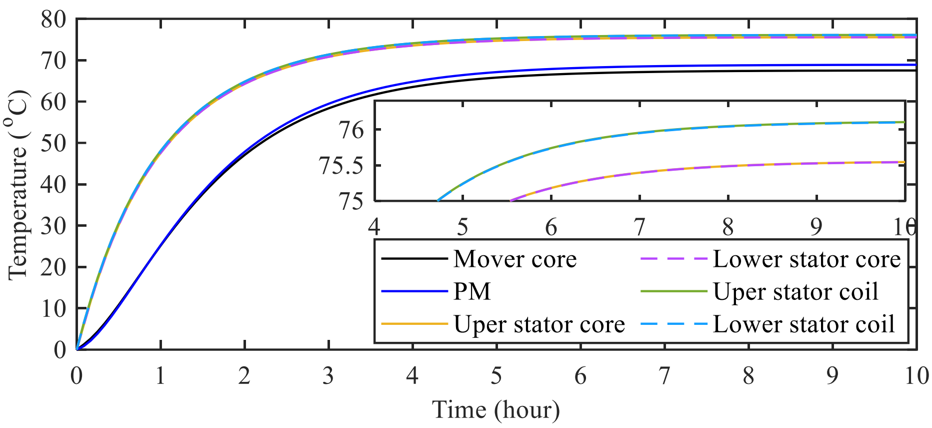

Figure 21. Thermal behavior at different time intervals.

7. Performance and Topology Comparison of Investigated DSSM-LOA with Traditional Designs of LA

Evaluation and comparison of the proposed DSSM-LOA with the state-of-the-art structures of linear actuators (LAs) with regards to performance and topology structure are accomplished in this section. First, the topological structure and moving type of the designs are elaborated on. Following that, a precise comparison is made between the proposed DSSM-LOA and the traditional MM-LAs. Furthermore, the parameters representing output parameters, such as MC and stroke, are contrasted. Following that, the MC per PM mass of the suggested DSSM-LOA and traditional LA designs are compared. Finally, a comparison concerning MC density and MC per overall volume of the LA is provided to elaborate on in-depth information and critical aspects of the proposed design.

Calculated and measured values of the parameters of the proposed DSSM-LOA and already built and examined topologies of LA are mentioned in Table 4. The stroke of the examined DSSM-LOA was 20mm, which was feasible for compressor application and quite a lot better compared to the other designs of LA, as shown in Table 4. Due to the less PM usage in the suggested design, the MC of the DSSM-LOA was lower than the design explored in [2], but the value of MC per mass of the recommended design was relatively better. Knowing that PM was the utmost costly component of LA designs, the proposed DSSM-LOA's MC per PM mass was superior to the other designs and higher than those indicated in Table 4. The design volume significantly impacted the actuator cost and motor constant, and the proposed DSSM-LOA had a higher MC density value, highlighting the significance of the proposed design.

Table 4. Mass comparison of different parts of the proposed and conventional of linear actuators.

Con-LA	Topology	Moving Type	Moving Mass (Kg)	Stroke (mm)	Peak Current (A)	Peak Force (N)	MC (N/A)	MC per PM Mass (N/Kg.Amp)	MC Density (N/mm^3.Amp)
[2]	Tubular	MM	0.9836	12	5	1000	200	263.744	2.95×10^{-4}
[7]	Tubular	MM	0.68	8.8	0.23	8	38	146.957	1.948×10^{-5}
[9]	Planar	MM	0.5462	12	5	600	120	312.500	1.016×10^{-4}
[18]	Tubular	MM	0.3482	14	1.75	99.02	56.6	254.799	2.08×10^{-4}
[23]	Tubular	MM	1.561008	10	5	215	48	147.761	6.23×10^{-5}
Proposed	Planar	MM	0.5372	20	5	660	132.2	443.500	1.12×10^{-4}

The investigated topology of DSSM-LOA used rectangular-shaped PMs and cores, which made the proposed design simple and low-cost. Rectangular PMs can be easily constructed with many small-dimensional components, and their proportions can be easily adjusted. Tubular LA fabrication is most challenging when making the laminations to lower the losses, due to the eddy current. DSSM-LOA was configured with rectangular parts that made laminations easy to assemble. A further advantage of the proposed DSSM-LOA was its open structure, which contributed to the improved thermal aspect of the actuator and the substitution of defective components.

8. Conclusions

This paper investigated rectangular-shaped DSS-MLOA, which provided linear oscillation in a feasible stroke range. The mover of the researched design was composed of end ferromagnetic materials, and axially magnetized PMs were sandwiched between the core materials. The investigated design had two coils within each stator that were magnetized in opposite directions to one another and the other stator coils. The optimal dimensions were selected based on the EM force after all the geometric parameters were optimized using the finite parametric sweep methodology. The end ferromagnetic materials' contributions were analyzed concerning magnetic flux lines linking to the mover from the stator. Mechanical design parameters of the investigated design and conventional design were compared in terms of the masses of different parts of the structure. The performance of the investigated design was examined and compared with a single stator design of the proposed design and with the conventional rectangular structures of the LA regarding static EM force, dynamic EM force, and cogging force. Finally, the DSSM-LOA was evaluated in terms of stroke, motor constant, motor constant per PM mass, and motor constant per overall volume of the actuator, and it showed a considerable improvement over conventional moving-magnet designs of LA. The performance indices, such as motor constant, motor constant per PM mass, and motor constant per overall volume of the suggested DSSM-LOA, were raised by 10.166 percent, 41.92 percent, and 10.23 percent when compared to the base design, namely Con-DS-LOA. According to the results of the FEM study, the suggested DSSM-LOA output parameters are suitable for compressor applications while maintaining sample structure and low cost. Furthermore, the experimental validation of the proposed design is the future direction of our study.

Author Contributions: Conceptualization, Z.A.; methodology, Z.A. and B.U.; software, Z.A.; validation, Z.A. and B.U.; resources, F.K., S.U. and I.S.; formal analysis, B.U., S.U. and I.S.; original draft preparation, Z.A.; visualization, B.U.; review and editing, B.U. and F.K.; supervision, F.K.; project administration, F.K., S.U. and I.S.; funding acquisition, S.U. and I.S. All authors have read and agreed to the published version of the manuscript.

Funding: This research received no external funding.

Data Availability Statement: Not applicable.

Conflicts of Interest: The authors declare no conflict of interest.

References

1. Chen, X.; Jiang, H.; Li, Z.; Liang, K. Modelling and measurement of a moving magnet linear motor for linear compressor. *Energies* **2020**, *13*, 4030. [CrossRef]
2. Ahmad, Z.; Hassan, A.; Khan, F.; Ahmad, N.; Khan, B.; Ro, J.-S. Analysis and design of a novel outer mover moving magnet linear oscillating actuator for a refrigeration system. *IEEE Access* **2021**, *9*, 121240–121252. [CrossRef]
3. Ahmad, Z.; Hassan, A.; Khan, F.; Lazoglu, I. Design of a high thrust density moving magnet linear actuator with magnetic flux bridge. *IET Electr. Power Appl.* **2020**, *14*, 1256–1262. [CrossRef]
4. Ahmad, A.; Ullah, B.; Ahmad, Z.; Liu, G.; Jawad, M. Performance Analysis of Tubular Moving Magnet Linear Oscillating Actuator for Linear Compressors. *Energies* **2022**, *15*, 3224. [CrossRef]
5. Jiang, H.; Liang, K.; Li, Z. Characteristics of a novel moving magnet linear motor for linear compressor. *Mech. Syst. Signal Process.* **2019**, *121*, 828–840. [CrossRef]
6. Akbar, S.; Khan, F.; Ahmad, Z.; Ullah, W.; Ullah, B.; Hussain, S. Design and experimental analysis of high electromagnetic force density moving magnet linear actuator with end ferromagnetic poles. *IET Electr. Power Appl.* **2022**, *16*, 1158–1168. [CrossRef]
7. Hassan, A.; Bijanzad, A.; Lazoglu, I. Dynamic analysis of a novel moving magnet linear actuator. *IEEE Trans. Ind. Electron.* **2016**, *64*, 3758–3766. [CrossRef]
8. Pompermaier, C.; Kalluf, K.; Zambonetti, A.; Da Luz, M.F.; Boldea, I. Small linear PM oscillatory motor: Magnetic circuit modeling corrected by axisymmetric 2-D FEM and experimental characterization. *IEEE Trans. Ind. Electron.* **2011**, *59*, 1389–1396. [CrossRef]
9. Jawad, M.; Haitao, Y.; Ahmad, Z.; Liu, Y. Design and analysis of a novel linear oscillating actuator with dual stator rectangular geometry. *Appl. Comput. Electromagn. Soc. J. (ACES)* **2021**, *36*, 1384–1392. [CrossRef]
10. Kim, K.; Park, H.; Jeong, S.; Jang, S.; Choi, J. Comparison of characteristics of permanent-magnet linear oscillating actuator according to laminated method of stator core. *IEEE Trans. Appl. Supercond.* **2016**, *26*, 1–4. [CrossRef]
11. Dai, J.; Zhao, Z.; Xu, S.; Wang, C.; Zhu, J.; Fan, X. Inhibition of iron loss of the inner yoke in electromagnetic linear actuator. *IET Electr. Power Appl.* **2019**, *13*, 419–425. [CrossRef]
12. Li, C.; Zou, H.; Cai, J.; Jiang, Y.; Guo, C. Dynamic behavior analysis of a moving coil oil-free linear compressor in refrigeration system. *Int. J. Refrig.* **2022**, *133*, 235–246. [CrossRef]
13. Bijanzad, A.; Hassan, A.; Lazoglu, I. Analysis of solenoid based linear compressor for household refrigerator. *Int. J. Refrig.* **2017**, *74*, 116–128. [CrossRef]
14. Mirić, S.; Küttel, P.; Tüysüz, A.; Kolar, J.W. Design and experimental analysis of a new magnetically levitated tubular linear actuator. *IEEE Trans. Ind. Electron.* **2018**, *66*, 4816–4825. [CrossRef]
15. Kim, C.-W.; Jang, G.-H.; Shin, K.-H.; Jeong, S.-S.; You, D.-J.; Choi, J.-Y. Electromagnetic design and dynamic characteristics of permanent magnet linear oscillating machines considering instantaneous inductance according to mover position. *IEEE Trans. Appl. Supercond.* **2020**, *30*, 1–5. [CrossRef]
16. Zhao, F.; Jiang, Y.; Yang, K.; Zhang, C.; Lian, W.; Wang, G. Comparison Study on High Force Density Linear Motors for Compressor Application. *Energies* **2021**, *14*, 7417. [CrossRef]

17. Zhang, H.; Jin, L.; Yu, H.; Xu, Z.; Leng, J.; Zhu, X.; Fang, S. Electromagnetic Design of Single-Phase Permanent Magnet Linear Oscillation Actuator Considering Detent Force Minimum. *IEEE Trans. Magn.* **2021**, *58*, 1–5. [CrossRef]
18. Sun, J.; Luo, C.; Xu, S. Improvement of tubular linear oscillating actuators by using end ferromagnetic pole pieces. *IEEE Trans. Energy Convers.* **2018**, *33*, 1686–1691. [CrossRef]
19. Mirić, S.; Giuffrida, R.; Bortis, D.; Kolar, J.W. Dynamic electromechanical model and position controller design of a new high-precision self-bearing linear actuator. *IEEE Trans. Ind. Electron.* **2020**, *68*, 744–755. [CrossRef]
20. Birbilen, U.; Lazoglu, I. Design and analysis of a novel miniature tubular linear actuator. *IEEE Trans. Magn.* **2018**, *54*, 1–6. [CrossRef]
21. Ghahfarokhi, P.S.; Podgornovs, A.; Kallaste, A.; Cardoso, A.J.M.; Belahcen, A.; Vaimann, T. The Oil Spray Cooling System of Automotive Traction Motors: The State of the Art. *IEEE Trans. Transp. Electrif.* **2022**, *9*, 428–451. [CrossRef]
22. Lindh, P.; Egorov, D.; Credo, A.; Pyrhönen, J. Thermal Management of an Electric Motor with Novel Materials. In Proceedings of the 2022 International Conference on Electrical Machines (ICEM), Valencia, Spain, 5–8 September 2022; pp. 1369–1375.
23. Immonen, P.; Ruuskanen, V.; Pyrhönen, J. Moving magnet linear actuator with self-holding functionality. *IET Electr. Syst. Transp.* **2018**, *8*, 182–187. [CrossRef]